Inductive Tuning of Fano-Resonant Metasurfaces Using Plasmonic Response of Graphene in the Mid-Infrared

S. Hossein Mousavi,[†,§] Iskandar Kholmanov,[‡,§] Kamil B. Alici,[†] David Purtseladze,[†] Nihal Arju,[†] Kaya Tatar,[†] David Y. Fozdar,[†] Ji Won Suk,[‡] Yufeng Hao,[‡] Alexander B. Khanikaev,[†] Rodney S. Ruoff,[‡] and Gennady Shvets*,[†]

[†]Department of Physics and Center for Nano and Molecular Science and Technology and [‡]Department of Mechanical Engineering and Materials and Science Program, The University of Texas at Austin, Austin, Texas 78712, United States

Ⓢ Supporting Information

ABSTRACT: Graphene is widely known for its anomalously strong broadband optical absorptivity of 2.3% that enables seeing its single-atom layer with the naked eye. However, in the mid-infrared part of the spectrum graphene represents a quintessential lossless zero-volume plasmonic material. We experimentally demonstrate that, when integrated with Fano-resonant plasmonic metasurfaces, single-layer graphene (SLG) can be used to tune their mid-infrared optical response. SLG's plasmonic response is shown to induce large blue shifts of the metasurface's resonance without reducing its spectral sharpness. This effect is explained by a generalized perturbation theory of SLG-metamaterial interaction that accounts for two unique properties of the SLG that set it apart from all other plasmonic materials: its anisotropic response and zero volume. These results pave the way to using gated SLG as a platform for dynamical spectral tuning of infrared metamaterials and metasurfaces.

KEYWORDS: Graphene, Fano resonances, optical modulation, plasmonic metamaterials, mid-infrared
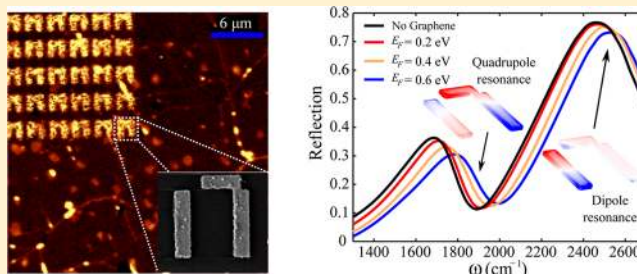
Artificial electromagnetic materials known as metamaterials (and their single-layer versions known as metasurfaces) have been experiencing an incredible surge in popularity because their optical response can be tailored to a variety of applications across the electromagnetic spectrum. Some of the most exotic phenomena recently demonstrated using electromagnetic metamaterials include negative refractive index, strong chirality, and indefinite electric permittivity.[1−5] Metamaterials manifesting these unusual optical properties are typically comprised of highly resonant plasmonic elements (e.g., split-ring resonators) that have a spectrally narrow response and high local field concentration. Owing to these properties, plasmonic metamaterials have recently emerged as a promising platform for a variety of applications that include chemical[6−9] and biological[10−13] sensing, nonlinear metatronics,[14] and light manipulation.[15]

The ability to actively control the resonant constitutive elements of metamaterials enables dynamic tunability of their optical response and can potentially expand the range of their applications even further. For example, applications requiring multiple metamaterial elements resonating at different frequencies, such as spatial light modulators,[16] broad-band delay lines,[15] and multispectral imaging/detection[12] would greatly benefit from dynamic tunability of bulk metamaterials and planar metasurfaces. A variety of approaches to achieving dynamic tunability have recently emerged. They rely on integrating metamaterials with various optically active materials

such as semiconductors with electrically/optically controlled free carriers,[17−21] liquid crystals,[22] magnetic materials,[23] quantum emitters,[24] and nonlinear media.[25] In this Letter, we experimentally demonstrate that blue-shifting tunability can be accomplished by placing chemically doped single-layer graphene (SLG) on top of a Fano-resonant mid-infrared (mid-IR) metasurface. SLG is particularly suitable for the mid-IR frequency range because of the combination of its strong plasmonic response and negligible loss. Further dynamic blue shifting can be accomplished by electrostatic gating.

To better understand the concept of frequency tuning it is instructive to represent a resonant metamaterial element (metamolecule) as an $L-C$ circuit possessing the resonance frequency $\omega_R = 1/(LC)^{1/2}$, where L and C are its effective inductance and capacitance,[26,27] respectively. Thus, the dynamical tuning is accomplished by changing the metamolecule's capacitance and/or inductance by placing an optically active component in its vicinity. For example, red-shifting of the resonant frequency by a thin dielectric or plasmonic layer can then by understood as increasing the capacitance due to the electric field expulsion from the layer. Indeed, adding fluid[6] or even a protein monolayer[12] to a metamaterial causes
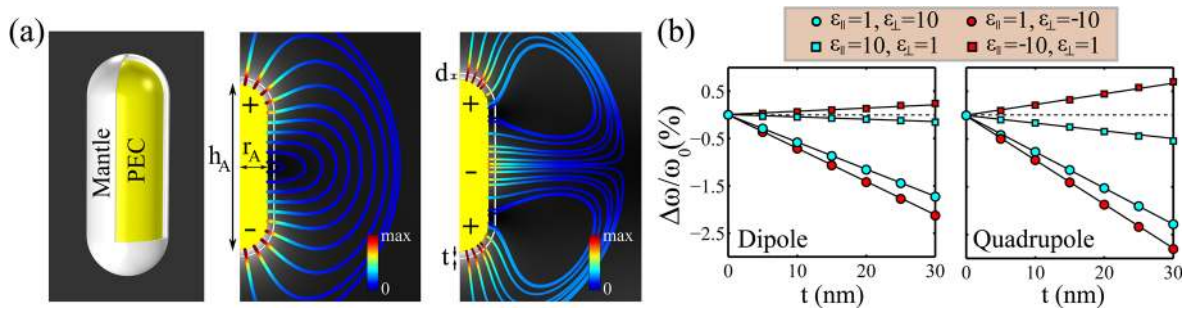
Figure 1. (a) (left) Schematics of a PEC antenna enveloped by an anisotropic conformal mantle of thickness t placed at a distance d from its surface. Field profiles of the electric dipole/quadrupole modes are shown in the middle/right panels. Lines of the electric field are color-coded according to its magnitude. (b) Spectral tuning of the dipole (left) and quadrupole (right) resonances as a function of the mantle thickness. Four types of anisotropic mantle were considered: (1) $\varepsilon_\parallel = 1$, $\varepsilon_\perp = 10$, (2) $\varepsilon_\parallel = 10$, $\varepsilon_\perp = 1$, (3) $\varepsilon_\parallel = 1$, $\varepsilon_\perp = -10$, and (4) $\varepsilon_\parallel = -10$, $\varepsilon_\perp = 1$. Markers, from eigenvalue simulations; solid lines, from eq 1. Antenna and mantle geometric parameters: $r_A = 500$ nm, $h_A = 3$ μm, and $d = 100$ nm.

measurable red-shifting that can be used for sensing. Achieving a blue shift would require reducing the inductance and is more challenging[19,28] because the capacitance increase due to field expulsion usually dominates.[28−30] This difficulty in blue-shifting metamaterial resonances has been recognized for some time,[18] and several approaches to decreasing L by optically induced switching to a different resonant mode of a metamaterial[18,19,28] have been recently demonstrated. Because these approaches rely on producing high densities of optically generated free carriers in semiconductors, they have been primarily restricted to the terahertz frequency range. Below, we describe an alternative approach to blue-shifting metamaterials' resonances in the mid-infrared part of the spectrum by enveloping them in a "zero-volume" nearly lossless plasmonic material: the SLG.

First, we develop a quantitative description of the metamaterial's tunability caused by enveloping a metamolecule by a thin optically anisotropic mantle[31] with an area S and thickness $t \ll \lambda_R$ as schematically shown in Figure 1, where λ_R is the resonant wavelength. To separate the contribution of the capacitive and inductive couplings, we further assume that the mantle conforms to the shape of the metamolecule and is made of an anisotropic material with in-plane and out-of-plane permittivities (defined with respect to the mantle's surface normal) given by $\varepsilon_\parallel$ and $\varepsilon_\perp$, respectively. According to the perturbation theory, the total resonance shift $\Delta\omega$ is given by the following sum[32,33]

$$\frac{\Delta\omega}{\omega} = \frac{t\int_S(1-\varepsilon_\parallel)|\mathbf{E}_\parallel|^2 dS}{W_0} - \frac{t\int_S\left(1-\frac{1}{\varepsilon_\perp}\right)|\mathbf{D}_\perp|^2 dS}{W_0} \quad (1)$$

where $W_0 = 2\int_V|\mathbf{E}|^2 \, dV$ is the stored electromagnetic energy of the uncovered metamolecule which, for simplicity, is assumed to be made of a perfect electric conductor (PEC), and the parallel/perpendicular components of $\mathbf{E}/\mathbf{D}$ (which are continuous across the mantle interface) are defined with respect to the mantle's normal. The first term in eq 1 is associated with inductive tuning, while the second term in eq 1 represents the effect of the capacitive tuning by electric field expulsion. Equation 1, which is valid for both single and arrayed metamolecules, predicts that the overall blue shift is possible only when the first term is larger than the second, that is, when the inductance's decrease due to the mantle's conductivity is greater that the capacitance's increase due to field expulsion.

To illustrate the challenge of achieving blue shifting of resonances, we have applied eq 1 to the simplest metamolecule: a mantle-cloaked PEC antenna shown in Figure 1a. The two

lowest modes of the antenna, electric dipolar and quadrupolar resonances, are shown in the middle and right panels of Figure 1a, respectively. Positive components of the permittivity tensor are assumed to be frequency independent while the negative components are assumed to have a Drude-like behavior such that $\varepsilon_{\parallel(\perp)}(\omega_0) = -10$, where ω_0 is the mode's eigenfrequency of the uncloaked antenna. Figure 1b shows the mantle-induced frequency shift of these modes as a function of the mantle thickness t for different signs of $\varepsilon_\parallel$ and $\varepsilon_\perp$. Markers indicate the results obtained from COMSOL eigenvalue solver involving an iteration procedure to account for the Drude-like material dispersion of the mantle's permittivity. Solid lines are calculated from 1 using the fields obtained from COMSOL simulations for the uncloaked antenna (see Supporting Information for details). Excellent agreement between perturbatively and exactly calculated frequency shifts validates eq 1.

Note that a mantle with only normal polarizability ($\varepsilon_\perp = \pm 10$, $\varepsilon_\parallel = 1$) always results in a capacitive red shift of the resonances that monotonically increases with the mantle's thickness. A mantle with only tangential polarizability ($\varepsilon_\perp = 1$, $\varepsilon_\parallel = \pm 10$) gives rise to an inductive red shift for $\varepsilon_\parallel > 0$ (dielectric response) and an inductive blue shift for $\varepsilon_\parallel < 0$ (plasmonic response). According to eq 1, the small magnitude of the blue shift is due to the electric field being mostly normal to the mantle. Because of the additive nature of the inductive and capacitive frequency shifts, a mantle made of an isotropic material red shifts antenna resonances regardless of the sign of $\varepsilon_\parallel = \varepsilon_\perp$. This demonstrates the challenge of achieving blue shifting using conventional (isotropic: $\varepsilon_\perp = \varepsilon_\parallel$) dielectric or plasmonic mantle materials.

According to eq 1 and Figure 1b, an anisotropic mantle with plasmonic tangential polarizability ($\varepsilon_\parallel < 0$) and vanishing perpendicular polarizability ($\varepsilon_\perp = 1$) always causes blue shifting. One such mantle is SLG: an effectively "zero-volume" plasmonic material with the tangential polarizability given by $t(\varepsilon_\parallel - 1) = (i\sigma/\omega)$, where graphene's surface conductivity is given by $\sigma(\omega) = \sigma_D(\omega) + \sigma_I(\omega)$. Here $\sigma_D(\omega)$ and $\sigma_I(\omega)$ originate from the intra- and interband transitions, respectively,[34−36] and are given by the following expressions that are valid in the low temperature limit

$$\sigma_{\rm D}(\omega) = \frac{ie^2}{\pi\hbar}\left\{\frac{E_{\rm F}}{\hbar(\omega + i\gamma)}\right\}$$

$$\sigma_{\rm I}(\omega) = \frac{ie^2}{4\pi\hbar}\left\{\ln\left|\frac{\hbar\omega - 2E_{\rm F}}{\hbar\omega + 2E_{\rm F}}\right| - i\pi\theta(\hbar\omega - 2E_{\rm F})\right\} \quad (2)$$

It follows from eq 2 that graphene's conductivity strongly depends on the value of its Fermi energy $E_{\rm F}$ which can be controlled by chemical doping and electrostatic gating.[37,38] The value of $E_{\rm F}$ is determined by the surface density of free carriers n according to $E_{\rm F} = \hbar|v_{\rm F}|(\pi n)^{1/2}$ where $|v_{\rm F}| = 1.1 \times 10^8$ cm s^{-1} is the Fermi velocity.[39] The intraband transitions (characterized by the collisional frequency $\gamma \ll \omega$) result in a low-loss plasmonic $[{\rm Im}(\sigma_{\rm D}) > 0]$ response of the SLG in mid-IR.[40] On the other hand, the interband transitions tend to reduce the plasmonic response and enhance losses for higher frequencies satisfying $\hbar\omega > 2E_{\rm F}$.

To illustrate the uniqueness of the mid-IR frequency range for low-loss graphene response, we plot in Figure 2 the ratio of
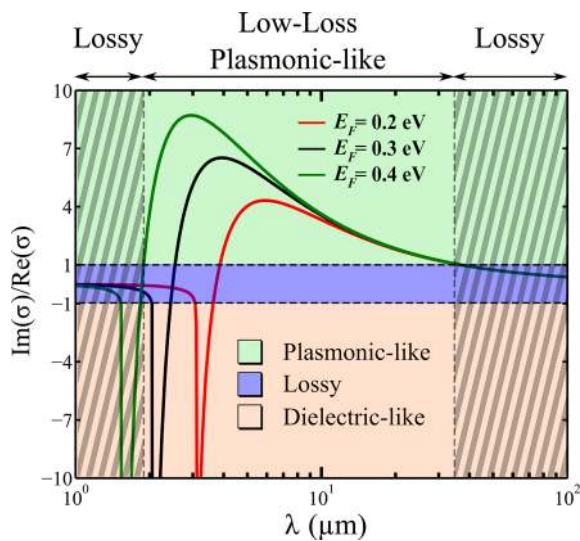

Figure 2. Optical response of moderately doped graphene in different spectral ranges: A mid-IR window, with dominantly plasmonic response, inside the entire optical spectrum with dominantly lossy behavior. Plasmonic and lossy regimes are shown by arrows on the top for a graphene with $E_{\rm F} = 0.4$ eV. A narrow spectral range at which graphene behaves as a dielectric occurs at $\omega = 2E_{\rm F}/\hbar$ inside the low-wavelength lossy regime. The graphene intraband scattering rate was assumed to be $\gamma = 269$ cm^{-1}.

the reactive (inductive or capacitive) to resistive conductivities of moderately doped SLG. Clearly, the large ratio ${\rm Im}(\sigma) \gg {\rm Re}(\sigma)$ is achieved only in the mid-IR frequency range ($\gamma \ll \omega < 2E_{\rm F}/\hbar$). Most of the earlier research on optical applications of graphene concentrated on either (i) far-IR and terahertz regimes[38,41,42] ($\omega < \gamma$), where considerable losses are caused by intraband transitions, or (ii) near-IR and visible ranges[43] ($\hbar\omega > 2E_{\rm F}$), where interband transitions also cause considerable losses. While earlier studies have demonstrated that graphene's resistive response in the near-IR and THz ranges can be profitably used for amplitude modulation,[38,43−45] these spectral ranges have limited appeal for low-loss spectral tuning of metamaterials. Although Figure 2 indicates that low-loss plasmonic response of graphene could potentially be extended into the near-IR region by doping graphene at high levels ($E_{\rm F} >$

0.5 eV), such high doping levels are challenging to achieve using the conventional back-gating configuration.[39]

Also in the mid-IR region, a study of graphene/metamaterial hybrid structures[46] has shown a lossy behavior from graphene, although according to the above discussion, graphene in this region should have exhibited a plasmonic response and have given rise to spectral tunability of the resonances. However, the observed predominantly lossy behavior is due to the structure design. This shows that deeper understanding of the interaction of graphene with the near-field of metamaterials is required in order to achieve spectral tunability of hybrid graphene/metamaterial systems.

To demonstrate the possibility of inductive tuning in the mid-IR due to plasmonic response of SLG, we utilized a Fano-resonant[15,47−55] metasurface (FRAM) exemplified by a two-dimensional periodic array of π-shaped plasmonic metamolecules comprised of three antennas shown in Figure 3a,b. This structure exhibits strong field enhancement and high-slope asymmetric Fano resonances[12,15,56] which were shown to be beneficial for biosensing and orientation characterization of protein monolayers.[12] The near-field coupling between the two vertical antennas results in the appearance of two modes with disparate quality factors. These modes are the low-Q dipolar and high-Q quadrupolar modes which have predominantly symmetric (right inset in Figure 4) and antisymmetric (left inset in Figure 4) distribution of surface charges on the vertical antennas, and are referred to[57,58] as "bright" and "dark" modes, respectively. Both the dipolar ($\omega_{\rm D} = 2430$ cm^{-1}) and quadrupolar ($\omega_{\rm Q} = 1770$ cm^{-1}) resonance frequencies are designed to occur in the mid-IR part of the spectrum by the appropriate choice of antenna dimensions. The interference between the two resonant pathways results in a typical asymmetric Fano feature in the spectrum shown in Figure 4. The strongest field enhancement in the gaps between the antennas[12,56] occurs at $\omega = \omega_{\rm Q}$.

The optical response of the FRAM can be described by the temporal coupled-mode theory,[12,59] which results in the complex reflectivity coefficient $r(\omega)$ of the metasurface which can be approximated by the double-Lorentzian function:[12]

$$r = \frac{A_{\rm D}}{i(\omega - \omega_{\rm D}) + \frac{1}{\tau_{\rm D}}} + \frac{A_{\rm Q}}{i(\omega - \omega_{\rm Q}) + \frac{1}{\tau_{\rm Q}}} \quad (3)$$

where $A_{\rm D}$ and $A_{\rm Q}$ are complex amplitudes of the corresponding modes proportional to their far-field coupling. The quality factors of the two resonances are related to their lifetimes $\tau_{\rm D(Q)}$ according to $Q_{\rm D(Q)} \equiv \omega_{\rm D(Q)}\tau_{\rm D(Q)}$.

The addition of a SLG perturbs the resonant frequencies of the modes according to $\tilde{\omega}_{\rm D(Q)} = \omega_{\rm D(Q)} + \Delta\tilde{\omega}_{\rm D(Q)}$, where the graphene-induced complex-valued spectral shift $\Delta\tilde{\omega}_{\rm D(Q)}$ is calculated by inserting graphene's conductivity given by $t(\varepsilon_\parallel - 1) = (i\sigma/\omega)$ into eq 1 and observing that the graphene's thickness t drops out from the final result

$$\Delta\tilde{\omega}_{\rm D(Q)} = \frac{\sigma}{i}\frac{\int_S |E_{\parallel {\rm D(Q)}}|^2 {\rm d}S}{W_{0{\rm D(Q)}}} \quad (4)$$

where $\vec{E}_{\parallel {\rm D(Q)}}$ is the tangential electric field of the respective mode at the SLG's surface. It follows from eq 4 that the addition of SLG causes (i) a spectral shift ${\rm Re}(\Delta\tilde{\omega}_{\rm D(Q)})$ of the resonant frequencies proportional to the imaginary part of graphene's surface conductivity $[{\rm Im}(\sigma)]$, and (ii) a change in the lifetime of the modes, defined by ${\rm Im}(\Delta\tilde{\omega}_{\rm D(Q)})$, proportional
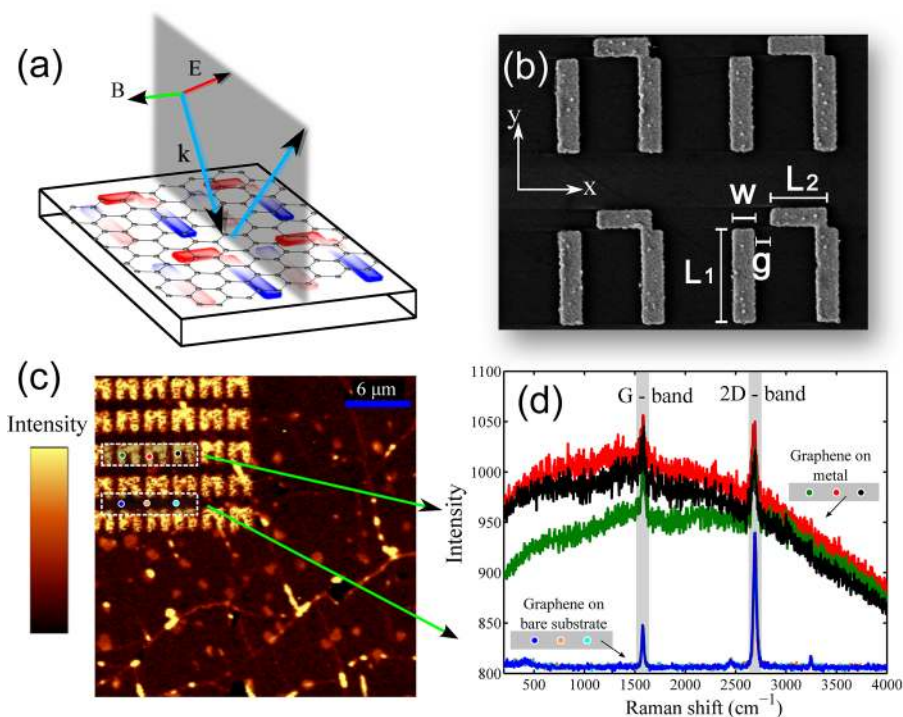
Figure 3. (a) Schematics of a monolayer graphene sheet on a Fano-resonant metasurface (FRAM). The incident polarization is parallel to the vertical antennas. (b) SEM image of the fabricated FRAM. (c) Raman map of the graphene transferred onto FRAMs using 488 nm wavelength laser excitation. Color shows the G-peak intensity. (d) Raman spectrum at six different locations on the metasurface: three spectra taken on the metallic antennas (red, black, and green) and three spectra (dark blue, light blue, and orange) taken on the bare quartz, all of which confirm the presence of high quality graphene.
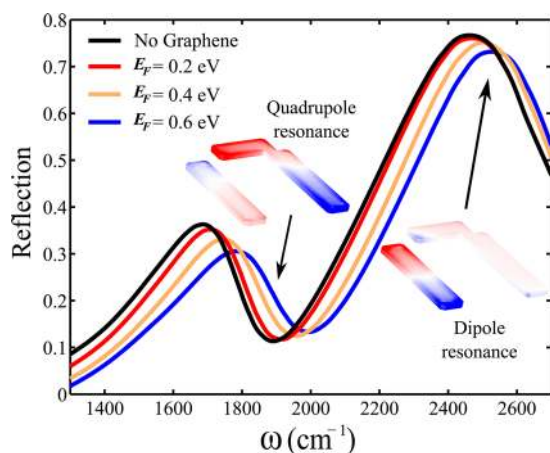

Figure 4. (a) Reflectivity spectrum from the metasurface without (black) and with graphene calculated using COMSOL FEM simulations. Insets: charge distribution on the metasurface at the dipolar (right) and the quadrupolar (left) resonances. Geometrical dimensions (see Figure 3 for definitions): $W = 275$ nm, $L_1 = 1.44$ μm, $L_2 = 815$ nm, and $g = 245$ nm; periodicities: $P_x = 2.05$ μm, and $P_y = 2.39$ μm. SLG is modeled as an infinitesimal conducting sheet in the $x-y$ plane at a distance $d = 5$ nm above the metasurface with intraband scattering rate $\gamma = 269$ cm^{-1}.

to the real part of the conductivity $[\text{Re}(\sigma)]$. In the mid-IR where, according to Figure 2, $\text{Im}(\sigma) \gg \text{Re}(\sigma)$, the presence of graphene mostly affects the spectral position of the modes rather than their lifetimes.

Note that, according to Figure 2, $\text{Im}(\sigma) > 0$ for moderately doped graphene, resulting in a blue shift of both resonances. A larger frequency shift is expected[43] for the quadrupolar mode

which is strongly confined to the metasurface. Note that the sign of the spectral shift due to SLG is opposite to that previously observed for protein monolayers tethered to the same metasurface.[12] The difference is attributed to plasmonic conductivity of graphene in contrast to the dielectric response of proteins.

Numerical calculations of the electromagnetic response of the metasurface with and without graphene were done with COMSOL. The simulated reflectivity spectrum $|r(\omega)|^2$ without graphene ($\sigma = 0$) shown in Figure 4 confirms that the structure exhibits Fano-like shape due to the interference between dipolar and quadrupolar resonances. Note that the dipolar resonance corresponds to the maximum of the broad reflectivity peak and the quadrupolar resonance is approximately located at the point of the highest slope of the reflectivity curve. The quality factors were found to be $Q_D \approx 3.9$ for the dipolar resonance and $Q_Q \approx 9.5$ for the quadrupolar resonance by fitting the reflectivity spectrum to eq 3. Next, graphene with three different values of the Fermi energy E_F was introduced into the COMSOL model. The graphene sheet on top of the metasurface was modeled by introducing a discontinuity in the tangential magnetic field: $-\hat{n} \times (\vec{H}_2 - \vec{H}_1) = (4\pi/c)\sigma\vec{E}$ across the SLG surface. SLG was assumed to be in the $x-y$ plane above the metasurface at a distance $d = 5$ nm. The resulting reflectivity spectra for $E_F = 0.2-0.6$ eV are shown in Figure 4. Indeed, as expected from the above theoretical results, the addition of the SLG results in a blue shift of both resonances. In addition to the blue shift, the quadrupolar resonance experiences a small drop in its intensity due to the decrease of its lifetime τ_Q by $\Delta\tau \approx \tau^2 \text{Im}(\Delta\tilde{\omega})$ due to graphene's finite resistivity. This dependence of the resonance position and the lifetime on the value of E_F suggests that the

doping level of graphene can be estimated spectroscopically as demonstrated below.

The experimental demonstration of SLG-induced inductive blue shifting of metamaterial resonances was carried out. First, two slightly different FRAM samples (S1 and S2) with geometric dimensions scaled by factor $\eta = 0.98$ were fabricated on the same quartz substrate using electron-beam lithography. Second, CVD-grown graphene[60] was transferred onto the metasurfaces using a dry transfer method.[61] Raman spectra obtained at different locations of the metasurfaces using a 488 nm wavelength laser are shown in Figure 3c,d. The spectra on the bare substrate and on the metallic antennas show pronounced G and 2D Raman-active bands of graphene. The small fraction of the G-mode to 2D-mode intensities indicates the presence of a high quality SLG on the metasurfaces. Finally, optical characterization of the structures was performed using a Thermo Scientific Continuum microscope coupled to a Nicolet 6700 FTIR Spectrometer. All spectroscopic measurements were carried out before and after graphene transfer with a p-polarized IR beam. The experimentally measured reflectivities for both samples are plotted in Figure 5 with (dashed lines) and
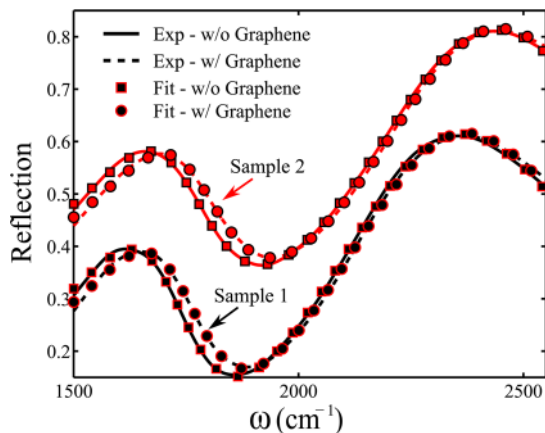

Figure 5. Experimentally measured reflectivity spectra for the two samples S1 (black) and S2 (red) before (solid curves) and after (dashed curves) graphene transfer. Markers: numerical fits to 3 are shown with a marker before (rectangles) and after (circles) graphene transfer. A vertical offset of 0.15 is introduced for sample S2 for clarity. Geometrical dimensions for S1: $W = 278$ nm, $L_1 = 1.47$ μm, $L_2 = 829$ nm, $g = 249$ nm, $P_x = 2.09$ μm, and $P_y = 2.44$ μm. All dimensions are scaled by $\eta = 0.98$ for S2. Gold thickness: 60 nm for S1 and S2.

without (solid lines) graphene. The spectral positions and quality factors of the dipolar and quadrupolar resonances before and after SLG transfer were determined by fitting the experimental reflectivity spectra to $R(\omega) \equiv |r(\omega)|^2$ calculated from eq 3. The results of the fits before/after SLG transfer are plotted in Figure 5 by rectangles/circles. As previously noted, the quadrupolar resonance was spectrally shifted by a larger amount $[\Delta\tilde{\omega}_{Q,S1} = (28.9 + 6.3i)$ cm^{-1} and $\Delta\tilde{\omega}_{Q,S2} = (30.3 + 6.2i)$ cm$^{-1}]$ than the dipolar resonance $[\Delta\tilde{\omega}_{D,S1} = (11.7 + 3.3i)$ cm^{-1} and $\Delta\tilde{\omega}_{D,S2} = (9.2 + 2.0i)$ cm$^{-1}]$ for both samples. Note that the magnitude of the spectral shift (close to 30 cm^{-1}) induced by a single atomic layer is considerably larger that the frequency shift of approximately 18 cm^{-1} induced by a 8 nm thick protein bilayer[12] in a similar metasurface. The result is even more remarkable in that only a small portion of the SLG overhanging between the two antennas, where the hotspot (maximal tangential electric field enhancement) for the

quadrupolar resonance is located,[15,56] is responsible for the shift. The extracted parameters enable us to conclude that the addition of a SLG mainly results in spectral blue shifting while only marginally affecting the lifetimes of the quadrupolar resonances $[\tau_{Q,S1}^{-1} = 171.2$ cm^{-1} and $\tau_{Q,S2}^{-1} = 177.4$ cm$^{-1}]$ of both samples.

To estimate the value of E_F for the unintentionally doped SLG in this experiment, we calculate the difference spectra $\Delta R(\omega) \equiv R_G - R_0$, where R_0 and R_G are the reflectivities before and after the graphene transfer. The experimentally measured difference spectra (normalized to the reflectivity peak R_Q at the low frequency range) are plotted in Figure 6 (solid lines). The
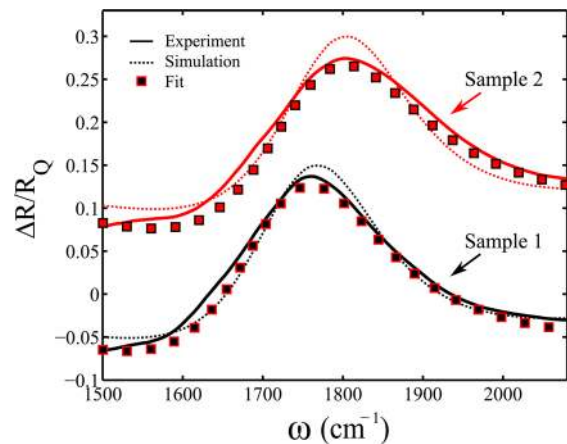

Figure 6. Reflectivity difference spectra $\Delta R \equiv R_G - R_0$ (with minus without graphene) for the two FRAM samples S1 (black) and S2 (red). Experimental (solid lines), double-Lorentzian fit (markers), and COMSOL simulations with $E_F = 0.2$ eV and $\gamma = 269$ cm^{-1} (dotted lines) are superimposed. A vertical offset of 0.15 is introduced for sample S2 for clarity.

maxima of ΔR are observed at the spectral positions ω_Q of the Fano resonance, where the maximal field intensity and the steepest slope in the reflectivity occur. The dashed lines in the same figure indicate the results of the COMSOL simulation assuming the graphene conductivity given by eq 2 with $E_F = 0.2$ eV and $\gamma = 269$ cm^{-1}.[35] The above value of E_F provides the best fit for both samples, and is consistent with that obtained from the Raman data collected from the graphene regions which are not in direct contact with the metal.

The results presented in Figure 6 pave the way for using SLG for dynamical control of transmission/reflection by infrared metasurfaces. In obtaining the experimental results presented above, we have relied on intrinsic doping of graphene and did not attempt to dynamically control E_F by electrostatic gating. Electrostatic modulation of E_F of the same order ($\pm 0.2-0.3$ eV)[46] appears feasible and, therefore, can be used for modulating the infrared response of metasurfaces.

In summary, we have developed a rigorous perturbation theory to describe inductive tuning of metamaterial resonances using graphene. On the basis of this theory, we have proposed an approach to achieve blue shift tunability of metasurfaces using the plasmonic response of graphene in the mid-IR. The blue shift is caused by the inductive coupling between metasurfaces and graphene and is theoretically shown to be controllable through electrostatic gating. We experimentally demonstrated that the transfer of chemically doped graphene onto the Fano-resonant metasurface alone results in the blue shift of the resonances ($\sim$30 cm^{-1}). The demonstrated

possibility to control optical response of the Fano-resonant metasurfaces through their inductive interaction with a monolayer graphene, combined with the possibility to control the Fermi level of graphene, paves the way for the next-generation tunable infrared optoelectronic devices.

■ ASSOCIATED CONTENT

Ⓢ Supporting Information

The details of the calculation of resonance-frequency shift using the first-order perturbation theory are given. This material is available free of charge via the Internet at http://pubs.acs.org.

■ AUTHOR INFORMATION

Corresponding Author
*E-mail: gena@physics.utexas.edu.

Author Contributions
§S.H.M. and I.K. contributed equally to this work.

Notes
The authors declare no competing financial interest.

■ ACKNOWLEDGMENTS

■ REFERENCES

(1) Smith, D. R.; Pendry, J. B.; Wiltshire, M. C. K. Metamaterials and Negative Refractive Index. *Science* **2004**, *305*, 788−792.

(2) Dolling, G.; Enkrich, C.; Wegener, M.; Soukoulis, C. M.; Linden, S. Observation of simultaneous negative phase and group velocity of light. *Science* **2006**, *305*, 892.

(3) Fedotov, V. A.; Papasimakis, N.; Plum, E.; Bitzer, A.; Walther, M.; Kuo, P.; Tsai, D. P.; Zheludev, N. I. Spectral Collapse in Ensembles of Metamolecules. *Phys. Rev. Lett.* **2010**, *104*, 223901.

(4) Yen, T. J.; Padilla, W. J.; Fang, N.; Vier, D. C.; Smith, D. R.; Pendry, J. B.; Basov, D. N.; Zhang, X. Terahertz Magnetic Response from Artificial Materials. *Science* **2004**, *303*, 1494−1496.

(5) Hoffman, A. J.; Alekseyev, L.; Howard, S. S.; Franz, K. J.; Wasserman, D.; Podolskiy, V. A.; Narimanov, E. E.; Sivco, D. L.; Gmachl, C. Negative refraction in semiconductor metamaterials. *Nat. Mater.* **2007**, *6*, 946−950.

(6) Liu, N.; Mesch, M.; Weiss, T.; Hentschel, M.; Giessen, H. Infrared Perfect Absorber and Its Application As Plasmonic Sensor. *Nano Lett.* **2010**, *10*, 2342−2348.

(7) Liu, N.; Tang, M. L.; Hentschel, M.; Giessen, H.; Alivisatos, A. P. Nanoantenna-enhanced gas sensing in a single tailored nanofocus. *Nat. Mater.* **2011**, *10*, 631.

(8) Lassiter, J. B.; Sobhani, H.; Fan, J. A.; Kundu, J.; Capasso, F.; Nordlander, P.; Halas, N. J. Fano Resonances in Plasmonic Nanoclusters: Geometrical and Chemical Tunability. *Nano Lett.* **2010**, *10*, 3184.

(9) Neumann, O.; Urban, A. S.; Day, J.; Lal, S.; Nordlander, P.; Halas, N. J. Solar Vapor Generation Enabled by Nanoparticles. *ACS Nano* **2012**, *7* (1), 42−49.

(10) Kabashin, A. V.; Evans, P.; Pastkovsky, S.; Hendren, W.; Wurtz, G. A.; Atkinson, R.; Pollard, R.; Podolskiy, V. A.; Zayats, A. V. Plasmonic nanorod metamaterials for biosensing. *Nat. Mater.* **2009**, *8*, 867.

(11) Aksu, S.; Yanik, A. A.; Adato, R.; Artar, A.; Huang, M.; Altug, H. High-Throughput Nanofabrication of Infrared Plasmonic Nano-antenna Arrays for Vibrational Nanospectroscopy. *Nano Lett.* **2010**, *10*, 2511.

(12) Wu, C.; Khanikaev, A. B.; Adato, R.; Arju, N.; Yanik, A. A.; Altug, H.; Shvets, G. Fano-resonant asymmetric metamaterials for ultrasensitive spectroscopy and identification of molecular monolayers. *Nat. Mater.* **2012**, *11*, 69−75.

(13) Cubukcu, E.; Zhang, S.; Park, Y.-S.; Bartal, G.; Zhang, X. Split ring resonator sensors for infrared detection of single molecular monolayers. *Appl. Phys. Lett.* **2009**, *95*, 043113.

(14) Chettiar, U. K.; Engheta, N. Optical Frequency Mixing through Nanoantenna Enhanced Difference Frequency Generation:Metatronic Mixer. *Phys. Rev. B* **2012**, *86*, 075405.

(15) Wu, C.; Khanikaev, A. B.; Shvets, G. Broadband Slow Light Metamaterial Based on a Double-Continuum Fano Resonance. *Phys. Rev. Lett.* **2011**, *106*, 107403.

(16) Chan, W. L.; Chen, H.-T.; Taylor, A. J.; Brener, I.; Cich, M. J.; Mittleman, D. M. A spatial light modulator for terahertz beams. *Appl. Phys. Lett.* **2009**, *94*, 213511.

(17) Degiron, A.; Mock, J. J.; Smith, D. R. Modulating and tuning the response of metamaterials at the unit cell level. *Opt. Express* **2007**, *15*, 1115−1127.

(18) Chen, H.-T.; O'Hara, J. F.; Azad, A. K.; Taylor, A. J.; Averitt, R. D.; Shrekenhamer, D. B.; Padilla, W. J. Experimental demonstration of frequency-agile terahertz metamaterials. *Nat. Photonics* **2008**, *2*, 295−298.

(19) Shen, N.-H.; Massaouti, M.; Gokkavas, M.; Manceau, J.-M.; Ozbay, E.; Kafesaki, M.; Koschny, T.; Tzortzakis, S.; Soukoulis, C. M. Optically Implemented Broadband Blueshift Switch in the Terahertz Regime. *Phys. Rev. Lett.* **2011**, *106*, 037403.

(20) Shadrivov, I. V.; Kapitanova, P. V.; Maslovski, S. I.; Kivshar, Y. S. Metamaterials Controlled with Light. *Phys. Rev. Lett.* **2012**, *109*, 083902.

(21) Jun, Y. C.; Gonzales, E.; Reno, J. L.; Shaner, E. A.; Gabbay, A.; Brener, I. Active tuning of mid-infrared metamaterials by electrical control of carrier densities. *Opt. Express* **2012**, *20*, 1903.

(22) Khatua, S.; Chang, W.-S.; Swanglap, P.; Olson, J.; Link, S. Active Modulation of Nanorod Plasmons. *Nano Lett.* **2011**, *11*, 3797−3802.

(23) Hand, T. H.; Cummer, S. A. Frequency tunable electromagnetic metamaterial using ferroelectric loaded split rings. *J. Appl. Phys.* **2008**, *103*, 066105−066105−3.

(24) Wu, X.; Gray, S. K.; Pelton, M. Quantum-dot-induced transparency in a nanoscale plasmonic resonator. *Opt. Express* **2010**, *18*, 23633−23645.

(25) Zharov, A. A.; Shadrivov, I. V.; Kivshar, Y. S. Nonlinear Properties of Left-Handed Metamaterials. *Phys. Rev. Lett.* **2003**, *91*, 037401.

(26) Lockyear, M. J.; Hibbins, A. P.; Sambles, J. R. Microwave Surface-Plasmon-Like Modes on Thin Metamaterials. *Phys. Rev. Lett.* **2009**, *102*, 073901.

(27) Navarro-Cía, M.; Beruete, M.; Agrafiotis, S.; Falcone, F.; Sorolla, M.; Maier, S. A. Broadband spoof plasmons and subwavelength electromagnetic energy confinement on ultrathin metafilms. *Opt. Express* **2009**, *17*, 18184−18195.

(28) Shen, N.-H.; Kafesaki, M.; Koschny, T.; Zhang, L.; Economou, E. N.; Soukoulis, C. M. Broadband blueshift tunable metamaterials and dual-band switches. *Phys. Rev. B* **2009**, *79*, 161102.

(29) Driscoll, T.; Kim, H.-T.; Chae, B.-G.; Kim, B.-J.; Lee, Y.-W.; Jokerst, N. M.; Palit, S.; Smith, D. R.; Ventra, M. D.; Basov, D. N. Memory Metamaterials. *Science* **2009**, *325*, 1518−1521.

(30) Langley, D.; Coutu, R. A., Jr.; Collins, P. J. Using Inductance as a Tuning Parameter for RF Meta-atoms. *Nano-Micro Lett.* **2012**, *4*, 103−109.

(31) Alù, A. Mantle cloak: Invisibility induced by a surface. *Phys. Rev. B* **2009**, *80*, 245115.

(32) Waldron, R. Perturbation theory of resonant cavities. *Proc. IEE - Part C: Monographs* **1960**, *107*, 272−274.

(33) Kottke, C.; Farjadpour, A.; Johnson, S. G. Perturbation theory for anisotropic dielectric interfaces, and application to subpixel

smoothing of discretized numerical methods. *Phys. Rev. E* **2008**, *77*, 036611.

(34) Jablan, M.; Buljan, H.; Soljacic, M. Plasmonics in graphene at infrared frequencies. *Phys. Rev. B* **2009**, *80*, 245435.

(35) Yan, H.; Xia, F.; Zhu, W.; Freitag, M.; Dimitrakopoulos, C.; Bol, A. A.; Tulevski, G.; Avouris, P. Infrared Spectroscopy of Wafer-Scale Graphene. *ACS Nano* **2011**, *5*, 9854−9860.

(36) Koppens, F. H. L.; Chang, D. E.; García de Abajo, F. J. Graphene Plasmonics: A Platform for Strong Light-Matter Interactions. *Nano Lett.* **2011**, *11*, 3370−3377.

(37) Wang, F.; Zhang, Y.; Tian, C.; Girit, C.; Zettl, A.; Crommie, M.; Shen, Y. R. Gate-Variable Optical Transitions in Graphene. *Science* **2008**, *320*, 206−209.

(38) Ju, L.; Geng, B.; Horng, J.; Girit, C.; Martin, M.; Hao, Z.; Bechtel, H. A.; Liang, X.; Zettl, A.; Shen, Y. R.; Wang, F. Graphene plasmonics for tunable terahertz metamaterials. *Nat. Nanotechnol.* **2011**, *6*, 630−634.

(39) Das, A.; Pisana, S.; Chakraborty, B.; Piscanec, S.; Saha, S. K.; Waghmare, U. V.; Novoselov, K. S.; Krishnamurthy, H. R.; Geim, A. K.; Ferrari, A. C.; Sood, A. K. Monitoring dopants by Raman scattering in an electrochemically top-gated graphene transistor. *Nat. Nanotechnol.* **2008**, *3*, 210−215.

(40) Thongrattanasiri, S.; Koppens, F. H. L.; García de Abajo, F. J. Complete Optical Absorption in Periodically Patterned Graphene. *Phys. Rev. Lett.* **2012**, *108*, 047401.

(41) Vakil, A.; Engheta, N. Transformation Optics Using Graphene. *Science* **2011**, *332*, 1291−1294.

(42) Bao, Q.; Zhang, H.; Wang, B.; Ni, Z.; Lim, C. H. Y. X.; Wang, Y.; Tang, D. Y.; Loh, K. P. Broadband graphene polarizer. *Nat. Photonics* **2011**, *5*, 411−415.

(43) Papasimakis, N.; Luo, Z.; Shen, Z. X.; De Angelis, F.; Di Fabrizio, E.; Nikolaenko, A. E.; Zheludev, N. I. Graphene in a photonic metamaterial. *Opt. Express* **2010**, *18*, 8353.

(44) Liu, M.; Yin, X.; Ulin-Avila, E.; Geng, B.; Zentgraf, T.; Ju, L.; Wang, F.; Zhang, X. A graphene-based broadband optical modulator. *Nature* **2011**, *474*, 64−67.

(45) Sensale-Rodriguez, B.; Yan, R.; Kelly, M. M.; Fang, T.; Tahy, K.; Hwang, W. S.; Jena, D.; Liu, L.; Xing, H. G. Broadband graphene terahertz modulators enabled by intraband transitions. *Nat. Commun.* **2012**, *3*, 780.

(46) Emani, N. K.; Chung, T.-F.; Ni, X.; Kildishev, A. V.; Chen, Y. P.; Boltasseva, A. Electrically Tunable Damping of Plasmonic Resonances with Graphene. *Nano Lett.* **2012**, *12*, 5202−5206.

(47) Fano, U. Effects of Configuration Interaction on Intensities and Phase Shifts. *Phys. Rev.* **1961**, *124*, 1866−1878.

(48) Miroshnichenko, A. E.; Flach, S.; Kivshar, Y. S. Fano resonances in nanoscale structures. *Rev. Mod. Phys.* **2010**, *82*, 2257−2298.

(49) Fedotov, V. A.; Rose, M.; Prosvirnin, S. L.; Papasimakis, N.; Zheludev, N. I. Sharp Trapped-Mode Resonances in Planar Metamaterials with a Broken Structural Symmetry. *Phys. Rev. Lett.* **2007**, *99*, 147401.

(50) Zhang, S.; Genov, D. A.; Wang, Y.; Liu, M.; Zhang, X. Plasmon-Induced Transparency in Metamaterials. *Phys. Rev. Lett.* **2008**, *101*, 047401.

(51) Verellen, N.; Sonnefraud, Y.; Sobhani, H.; Hao, F.; Moshchalkov, V. V.; Dorpe, P. V.; Nordlander, P.; Maier, S. A. Fano Resonances in Individual Coherent Plasmonic Nanocavities. *Nano Lett.* **2009**, *9*, 1663−1667.

(52) Fan, J. A.; Bao, K.; Wu, C.; Bao, J.; Bardhan, R.; Halas, N. J.; Manoharan, V. N.; Shvets, G.; Nordlander, P.; Capasso, F. Fano-like Interference in Self-Assembled Plasmonic Quadrumer Clusters. *Nano Lett.* **2010**, *10*, 4680−4685.

(53) Fan, J. A.; Wu, C.; Bao, K.; Bao, J.; Bardhan, R.; Halas, N. J.; Manoharan, V. N.; Nordlander, P.; Shvets, G.; Capasso, F. Self-Assembled Plasmonic Nanoparticle Clusters. *Science* **2010**, *328*, 1135−1138.

(54) Luk'yanchuk, B.; Zheludev, N. I.; Maier, S. A.; Halas, N. J.; Nordlander, P.; Giessen, H.; Chong, C. T. The Fano resonance in plasmonic nanostructures and metamaterials. *Nat. Mater.* **2010**, *9*, 707−715.

(55) Mousavi, S. H.; Khanikaev, A. B.; Shvets, G. Optical properties of Fano-resonant metallic metasurfaces on a substrate. *Phys. Rev. B* **2012**, *85*, 155429.

(56) Alonso-Gonzalez, P.; Schnell, M.; Sarriugarte, P.; Sobhani, H.; Wu, C.; Arju, N.; Khanikaev, A.; Golmar, F.; Albella, P.; Arzubiaga, L.; Casanova, F.; Hueso, L. E.; Nordlander, P.; Shvets, G.; Hillenbrand, R. Real-Space Mapping of Fano Interference in Plasmonic Metamolecules. *Nano Lett.* **2011**, *11*, 3922−3926.

(57) Fan, J. A.; Bao, K.; Wu, C.; Bao, J.; Bardhan, R.; Halas, N. J.; Manoharan, V. N.; Shvets, G.; Nordlander, P.; Capasso, F. Fano-Like Interference in Self-Assembled Plasmonic Quadrumer Clusters. *Nano Lett.* **2010**, *10*, 4680.

(58) Fan, J. A.; Wu, C.; Bao, K.; Bao, J.; Bardhan, R.; Halas, N. J.; Manoharan, V. N.; Nordlander, P.; Shvets, G.; Capasso, F. Self-Assembled Plasmonic Nanoparticle Clusters. *Science* **2010**, *328*, 1135.

(59) Haus, H. A. *Waves and Fields in Optoelectronics*; Prentice Hall: New York, 1983.

(60) Li, X.; Cai, W.; An, J.; Kim, S.; Nah, J.; Yang, D.; Piner, R.; Velamakanni, A.; Jung, I.; Tutuc, E.; Banerjee, S. K.; Colombo, L.; Ruoff, R. S. Large-Area Synthesis of High-Quality and Uniform Graphene Films on Copper Foils. *Science* **2009**, *324*, 1312−1314.

(61) Suk, J. W.; Kitt, A.; Magnuson, C. W.; Hao, Y.; Ahmed, S.; An, J.; Swan, A. K.; Goldberg, B. B.; Ruoff, R. S. Transfer of CVD-Grown Monolayer Graphene onto Arbitrary Substrates. *ACS Nano* **2011**, *5*, 6916−6924.